Nuclear Inst. and Methods in Physics Research, A 1053 (2023) 168387

Contents lists available at ScienceDirect

Nuclear Inst. and Methods in Physics Research, A

journal homepage: www.elsevier.com/locate/nima

Full Length Article

Influence of temperature on measurements of the Two Photon Absorption – Transient Current Technique in silicon planar detectors using a 1550 nm femtosecond fibre laser

S. Pape [a,b,*], E. Currás [a], M. Fernández García [c], M. Moll [a], M. Wiehe [a]

[a] CERN, Switzerland
[b] TU Dortmund University, Germany
[c] Instituto de Física de Cantabria (CSIC-UC), Spain

ARTICLE INFO

Keywords:
Solid state detectors
Solid state detector characterisation
Two Photon Absorption-Transient Current Technique

ABSTRACT

The effect of temperature on the excess charge carrier generation and collection, injected using two photon absorption at a wavelength of 1550 nm, is investigated in a 285 µm thick, p-type silicon planar detector, with a bulk resistivity of 3.7 kΩ cm. Charge collection measurements are performed for temperatures between −20 °C to 20 °C. The collected charge decreases by about 8% when the temperature is lowered from 20 °C to −20 °C, which is linked to a decreasing excess charge carrier generation. Further, a decreasing time over threshold is observed for decreasing temperatures, which is associated to an increasing charge carrier mobility.

1. Introduction

The Two Photon Absorption-Transient Current Technique (TPA-TCT) was developed to characterise semiconductor detectors with a three dimensional resolution. Femtosecond pulse lasers, with wavelength beyond the linear, but within the quadratic absorption regime are used (ca. 1200 nm $\leq \lambda \leq$ 2300 nm), to only generate excess charge carriers by the process of two photon absorption [1,2]. This allows to generate excess charge carriers in a confined volume around the focus that can be shifted through the device under test (DUT) to obtain the three dimensional resolution. The technique is widely used within the field of silicon detector characterisation [1,3–6], but so far a dedicated study about the influence of temperature was never performed. This study is especially important with respect to measurements of irradiated devices, as they are typically operated at low temperatures, to cope with the increased leakage current after irradiation [7].

2. Experimental setup

The used TPA-TCT setup is schematically shown in Fig. 1. It uses a fibre laser with a pulse width of 430 fs and a central wavelength of 1550 nm. The laser source is the LFC1500X FYLA laser module [8] and provides a pulse energy of 10 nJ with a seed frequency of 8.2 MHz. The pulse energy is adjusted by a neutral density filter and the frequency is picked by an acousto-optic modulator inside the "Pulse management" module. The laser system is described in great detail in [9]. For the here presented study, a pulse frequency of 1 kHz is used.

The laser light propagates in open space towards a Faraday cage, which is used for electromagnetic shielding. Furthermore, it is continuously flushed with dry air to establish a dry ambient, to avoid freezing and condensation at the DUT. The light is guided into the Faraday cage and traverses a highly focusing objective with a numerical aperture of 0.5, which focuses the laser light onto the DUT. It should be noted that spherical aberration occurs due to the mismatch in refractive indices between silicon and air that can elongate the volume of charge deposition. However, for the used objective it is found that a constant charge deposition throughout the full depth of a 300 µm thick silicon device is provided, which ensures that the change in the beam parameters due to spherical aberration is below the measurement sensitivity and therefore negligible. Following the procedure described in Ref. [2], the beam parameters are measured with the knife-edge technique. It is found for the present settings that the objective focuses the laser beam to a beam waist of $w_0 = (1.63 \pm 0.11)\,\mu m$ and a Rayleigh length in silicon of $z_R = (13.07 \pm 1.05)\,\mu m$. Therefore, the objective confines the volume of charge generation to about $\frac{4}{3}\pi(1.63\,\mu m)^2 \cdot 13.07\,\mu m \approx 145\,\mu m^3$ around the focal spot.

The DUT is glued with conductive silver epoxy to the metal contact of a ceramic printed circuit board (PCB). The temperature at the DUT is monitored with a Pt1000 thermistor, which is placed < 4 mm away from the DUT. The PCB is mounted and thermally coupled to a copper chuck, which is in thermal contact with a Peltier element. The hot side of the Peltier element is actively cooled by a Huber Chiller [10]. During the measurements, the temperature varies less than 0.1 K. The temperature

* Corresponding author at: CERN, Switzerland.
E-mail address: sebastian.pape@cern.ch (S. Pape).

https://doi.org/10.1016/j.nima.2023.168387
Received 20 January 2023; Received in revised form 19 April 2023; Accepted 19 May 2023
Available online 26 May 2023

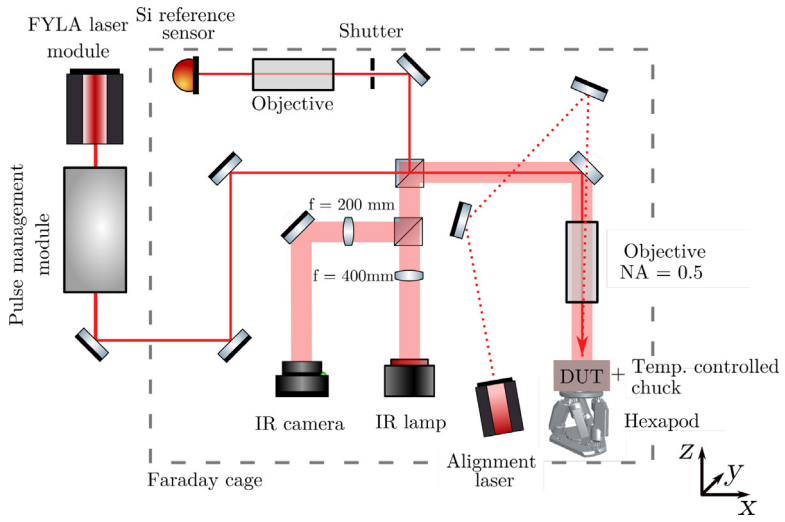

Fig. 1. Schematic drawing of the used TPA-TCT setup.

Table 1
Details of the used sensor.

Producer	Production run	Bulk type	Active thickness [µm]	Depletion voltage [V]	C_{end} [pF]	Bulk resistivity [kΩ cm]
CNM	7859	p-type	(282.7 ± 3.8)	27	4.06	3.7

controlled chuck is sitting on a HXP50-MECA high precision hexapod, which allows movement in all three dimensions and rotation around all axes. The rotation is used to correct for tilt between the xy-plane and the DUT, to ensure an orthogonal illumination. Details on the used tilt correction method are given in Section 3 or can be found in [2,11], along with more details on the used TPA-TCT setup. A red laser diode is used for the rough alignment of the DUT and an infrared microscope, which contains an infrared lamp (IR lamp) and an infrared camera (IR camera), is used for the fine alignment. The infrared microscope enables to live picture the DUT and the laser spot below the objective, which is especially useful to find references at the DUT. All in-depth scans are performed in the central position of the DUT.

Two different amplifiers are available to amplify signals from the DUT: first, a broadband CIVIDEC C2-TCT amplifier with a gain of 40 dB and a bandwidth of 10 kHz–2 GHz, which is optimised to obtain the pulse shape and second, a charge sensitive CIVIDEC Cx-L amplifier with a gain of 14.6 mV/fC that is optimised for charge collection measurements [12]. The DUT is biased and readout at the p-side (top) via the amplifier. The waveforms are recorded with the Agilent DSO9254A oscilloscope, which provides an upper bandwidth limit of 2.5 GHz and a sampling rate of 20 GS/s. The waveform is acquired 256 times and the averaged waveform is saved, to reduce the noise level.

The here presented study is performed on a ⟨100⟩ silicon p-type planar detector, fabricated in run 7859 by CNM [13]. Details of the DUT are shown in Table 1. The used electronics are expected to be suitable, because the readout of the detector introduces an RC ($R_{\text{system}} = 50\,\Omega$ and $C_{\text{end}} = 4.06\,\text{pF}$) with a high cut off frequency at about 800 MHz. For the presented measurements a bias voltage of 100 V is used, which is well above the device's full depletion voltage. The electric field is low enough to avoid any electric field related influences to the optical properties, i.e. the Franz-Keldysh effect is negligible for the used bias voltage [14]. The active thickness is extracted from an in-depth TPA-TCT scan as (282.7 ± 3.8) µm, which is in good agreement with the nominal value of 285 µm given by the producer.

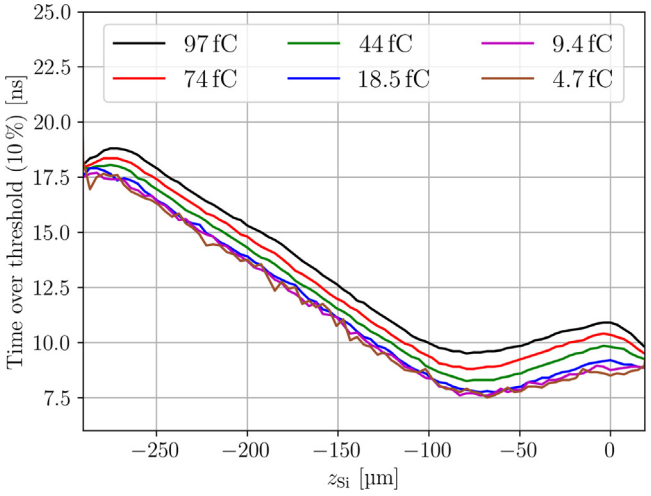

Fig. 2. The time the waveform is over 10% of its maximum against the device depth for different laser intensities. The laser intensity is given in the amount of the collected charge. The bias voltage is 100 V and the temperature is 20 °C. The back (top) side of the DUT is located at $z_{\text{Si}} = 0$ ($z_{\text{Si}} \approx -283$ µm).

3. Experimental results

In the following, the experimental results of the temperature study are presented. At the DUT position, laser pulse energies up to 1 nJ are achieved, which generate high enough charge carrier densities to excite an electron–hole plasma inside silicon. The plasma shields the contained charge carriers from the external electric field of the DUT and leads to a higher collection time [15,16]. To avoid the influence of plasma, in-depth scans at different intensities are performed to check for an increasing collection time. The result of this measurement is shown in Fig. 2, where the time over threshold (ToT) is measured against the device depth for different intensities. As a ToT, the time, the signal is above a threshold of 10% of its maximal amplitude, is used. For intensities > 18.5 fC an increased ToT is observed, which is linked to plasma effects.

3.1. Influence on the charge collection time

To study the influence of temperature on the collection time, in-depth scans with illumination from the front side are performed in the

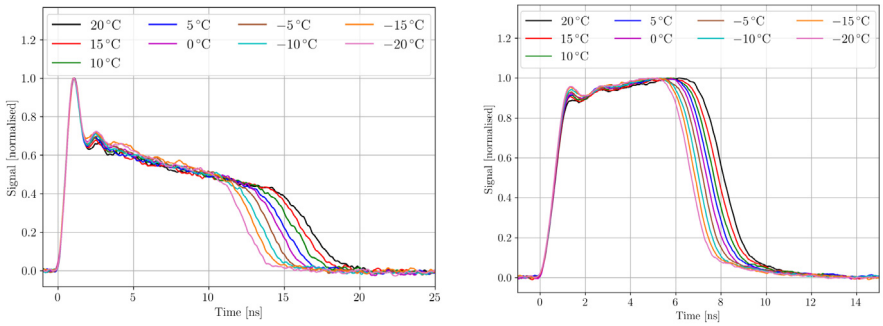

Fig. 3. Normalised induced current signals for different temperatures taken with a bias voltage of 100 V and a laser intensity corresponding to 18.5 fC. (a) and (b) are recorded for a charge deposition at the top side and a charge deposition at the back side, respectively.

centre position of the DUT at different temperatures. A laser intensity below the plasma regime is used and the CIVIDEC C2-TCT amplifier is taken. The measurement was started at a temperature of −20 °C and increased in 5 °C steps until 20 °C was reached. Following [2,11], in-depth scans were performed in a 3 × 3-grid and the position of the surface was extracted from each of the in total 9 scans individually. This allows to measure the tilt between the DUT and the laser beam. The tilt in this specific measurement campaign is $-1.1\,° \leq u \leq -1.06\,°$ and $0\,° \leq v \leq 0.08\,°$, where u (v) is the angle between the DUT and the y-axis (x-axis) of the coordinate system in Fig. 1. The tilt correction procedure was performed for each temperature step individually, to also correct any tilt induced by thermal expansion. It should be noted that gluing of the DUT and the PCB influence the tilt, wherefore it can be different for different samples. The alignment procedure takes about 20 min, which is enough time for the setup to reach the thermal equilibrium. Fig. 3 shows normalised induced current signals at different temperature and for two different deposition depths: one at the top side 3(a) and one at the back side 3(b). It can be seen that the collection time decreases for decreasing temperatures, due to the increasing charge carrier mobility. Further, due to the slope in the signal the dominance of either holes 3(a) or electrons 3(b) is well distinguishable. Fig. 4 shows the ToT against the device depth for an intensity corresponding to 18.5 fC at 20 °C for temperatures of 20 °C, 0 °C, and −20 °C. The ToT decreases with temperature, which is related to an increasing charge carrier mobility. Due to a shrinking phonon population, less scattering of the charge carriers occurs and thus, the charge carrier mobility increases [17]. The top side interface of the device is at $z_{\mathrm{Si}} \approx -283\,\mu\mathrm{m}$, and the back side interface is at $z_{\mathrm{Si}} = 0$. The DUT is a p-type device, wherefore electrons are collected at the top side and holes are collected at the back side electrode. The ToT at $z_{\mathrm{Si}} = 0$ origins from the electrons that traverse the full bulk, as the holes only need to drift a short distance towards their collecting electrode and are almost immediately collected. For decreasing z_{Si} values the electrons need to drift less and less distance towards their collecting electrode, which results in a decreasing ToT. This trend continuous until electrons and holes need the same collection time ($z_{\mathrm{Si}} \approx -70\,\mu\mathrm{m}$), which leads to a minimum in the ToT profile. Afterwards, the ToT increases, as holes start to dominate the waveform. The maximum ToT of holes exceeds the maximum ToT of electrons, because holes have a lower mobility [18]. The ToT reaches its maximum value at the top interface at $z_{\mathrm{Si}} = -285\,\mu\mathrm{m}$. There is no support wafer below the active volume and the back side of the DUT is not metallised. The difference in refractive indices of silicon ($n_{\mathrm{Si},20\,°\mathrm{C}} = 3.4757$ [19]) and air ($n_{\mathrm{air},20\,°\mathrm{C}} = 1$) leads to a reflection, which leads to a mirrored image for $z_{\mathrm{Si}} > 0$ [20]. For the investigated temperature range and the used bias voltage of 100 V, the holes mobility increases more with temperature than the electron mobility [21], wherefore the ToT of the electron dominated part ($-70\,\mu\mathrm{m} < z_{\mathrm{Si}} < 0$) decreases less with temperature than the holes dominated part.

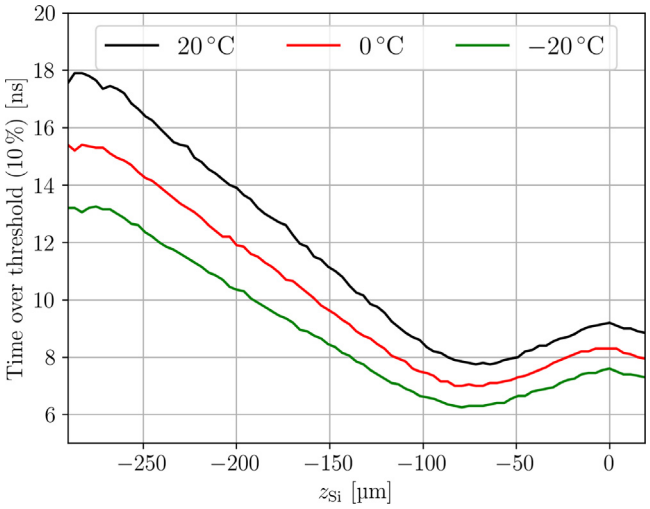

Fig. 4. The time the waveform is over 10% of its maximum against the device depth for different temperatures. A laser intensity corresponding to 18.5 fC and a bias voltage of 100 V are used.

3.2. Influence on the charge generation

The influence of temperature on the charge generation is investigated with a long term measurement, where the laser's focal point was positioned in the middle of the DUT and the stage is not moved during a measurement at a given temperature. A charge sensitive amplifier is used to increase the precision on the collected charge, and in total five thousand waveforms are recorded, with a time of 5 s between each acquisition, which results in a total measurement time of about 8.5 h for one temperature step. Such long measurements are needed to correct for potential laser pulse duration fluctuations, which were observed for short term measurements and lead to incomparable charge collections. These fluctuations vary the generated excess charge by up to 20 % and they could not be fully compensated by the energy monitor. Only data recorded during stable operation is used to ensure that a comparable excess charge is generated to improve the signal to noise ratio of the measurement. Fig. 5 shows the results of the measurement, where the collected charge is normalised with the charge collected at 20 °C and shown for different temperatures. Furthermore, to compare the influence on the TPA-TCT with the infrared single photon absorption (SPA) TCT, a charge collection measurement at the same temperatures, a comparable generated charge and the same DUT is performed in a setup with a 1064 nm infrared laser is as well shown. The SPA-TCT setup is well described in the Refs. [22,23]. It can be seen that the charge collection decreases for both measurements: the

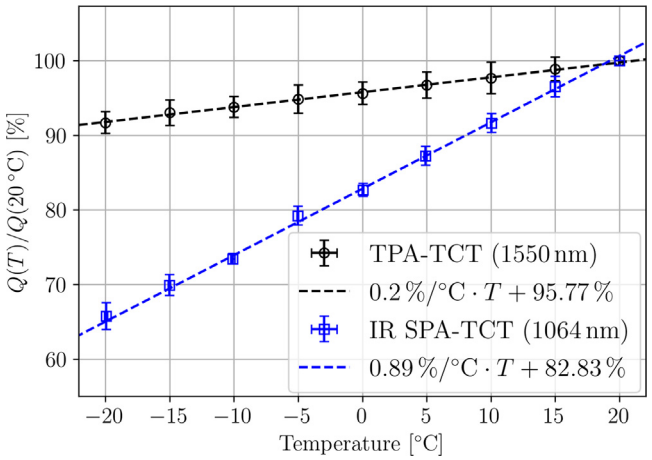

Fig. 5. Collected charge normalised with the charge collected at 20 °C at different temperatures, measured with infrared SPA-TCT and TPA-TCT. About 9.4 fC is generated at 20 °C for TPA-TCT, and a comparable charge is generated for the infrared SPA-TCT. The DUT is biased to 100 V. Linear functions are fitted towards the data.

charge collection of SPA-TCT decreases by (35.0 ± 0.4) % and the charge collection of TPA-TCT decreases by (8.3 ± 1.4) %. A linear fit is used for the interpolation of the charge collection of the TPA-TCT and the SPA-TCT measurement, as it appears linear in the used temperature range. It should be noted that the general temperature dependence for both measurements is non-linear.

The decreasing collected charge is a direct result of a decreasing generated charge, which is elaborated in the following for the TPA-TCT results. The generated charge of TPA is proportional to:

$$Q_{\mathrm{TPA}}(T) \propto n_{\mathrm{Si}}(T)\beta_2(T),$$

with the refractive index of silicon n_{Si} and the quadratic absorption coefficient β_2 [2]. Linear and higher order absorption can potentially contribute to the charge generation, but an intensity scan showed a purely quadratic relation between the intensity and the generated charge, which confirms that TPA is the dominating contribution and other contributions can be neglected. The temperature dependence of the charge generation can only origin from changes of the refractive index and the quadratic absorption coefficient. The refractive index decreases with temperature, but for the used temperature range the decrease is only about 0.2% [19]. This decrease of the refractive index excludes that the change in reflectivity of the material is above the sensitivity of the used method and ensures that a comparable amount of light intensity is involved in the charge generation process for all used temperatures. It follows that the decrease of the refractive index is too low to explain the observed temperature dependence and thus the quadratic absorption coefficient must be the dominating contribution for the temperature dependence of the charge generation in the investigated temperature regime. Ref. [24] reports a decreasing quadratic absorption coefficient of silicon from 17 °C to −23 °C by (12.0 ± 2.6) %, which agrees within the errors with the here reported decrease of the collected charge. This suggests that the collection of the charge itself is not influenced by the temperature, but only the charge generation. The decreasing absorption coefficient depends on the energy band gap and the phonon population, which both depend on the temperature: the energy band gap increases [25] and the phonon population decreases with temperature [26]. However, the energy band gap increases only by about 1 meV for the investigated temperature regime and is below the sensitivity of the used method. Consequently, the observed decrease of the absorption coefficient, i.e. charge generation, is dominated by the shrinking phonon population. For the SPA-TCT, the generated charge is proportional to:

$$Q_{\mathrm{SPA}}(T) \propto (1 - \exp(-\alpha(T) \cdot d)),$$

with the linear absorption coefficient α and the active device thickness d. Again, the refractive index and energy band gap can be considered as constant for the investigated temperature range. The expected decrease in charge generation, using the absorption coefficient of intrinsic silicon for the given temperature from Ref. [27], is $Q_{\mathrm{SPA}}(-20\ °C)/Q_{\mathrm{SPA}}(20\ °C) \approx (57.1 \pm 2.9)$ %. The consideration of reflection at the top and back surface changes the expected charge generation at −20 °C to (59.6 ± 2.8) % of the charge collection at 20 °C, which is (5.4 ± 2.8) % less than the observed value.

4. Conclusion

A compact TPA-TCT setup with a 1550 nm fs-pulsed fibre laser was used to investigate the influence of temperature on the TPA-TCT measurement technique. In-depth and charge collection scans of a 283 µm thick, p-type planar detector at different temperatures were performed. A decreasing charge collection time was observed, which is linked to an increasing charge carrier mobility. Furthermore, it is found that the collected charge reduces by (8.3 ± 1.4) %, from 20 °C to −20 °C, which is connected to a decreasing quadratic absorption coefficient and hence a decreasing charge carrier generation. It was shown that the decrease of the quadratic absorption coefficient for a wavelength of 1550 nm is much smaller than for the linear absorption coefficient of a 1064 nm ps-pulsed laser, which is in the DUT about (35.0 ± 0.4) %. The presented method, to investigate the charge carrier generation, could be extended to other temperature regimes and wavelength.

Declaration of competing interest

The authors declare that they have no known competing financial interests or personal relationships that could have appeared to influence the work reported in this paper.

Data availability

Data will be made available on request.

Acknowledgements

This project was performed within the framework of RD50 and has received funding from the European Union's Horizon 2020 Research and Innovation programme under GA no 101004761 (AIDAinnova), the Wolfgang Gentner Program of the German Federal Ministry of Education and Research (grant no. 05E18CHA), and the CERN, Switzerland Knowledge Transfer Fund, through a grant awarded in 2017.

References

[1] M. Fernández García, R. Jaramillo Echeverría, M. Moll, R. Montero Santos, R. Palomo Pinto, I. Vila, M. Wiehe, High resolution 3D characterization of silicon detectors using a two photon absorption transient current technique, Nucl. Instrum. Methods Phys. Res. A 958 (2020) http://dx.doi.org/10.1016/j.nima.2019.162865.

[2] M. Wiehe, M. Fernández García, M. Moll, R. Montero, F.R. Palomo, I. Vila, H. Muñoz-Marco, V. Otgon, P. Pérez-Millán, Development of a tabletop setup for the transient current technique using two-photon absorption in silicon particle detectors, IEEE Trans. Nucl. Sci. 68 (2) (2021) 220–228, http://dx.doi.org/10.1109/TNS.2020.3044489.

[3] S. Pape, E. Currás, M. Fernández García, M. Moll, R. Montero, F. Palomo, I. Vila, M. Wiehe, C. Quintana, First observation of the charge carrier density related gain reduction mechanism in LGADs with the two photon absorption-transient current technique, Nucl. Instrum. Methods Phys. Res. A 1040 (2022) http://dx.doi.org/10.1016/j.nima.2022.167190.

[4] S. Pape, E. Currás, M. Fernández García, M. Moll, Techniques for the investigation of segmented sensors using the two photon absorption-transient current technique, Sensors 23 (2) (2023) http://dx.doi.org/10.3390/s23020962.

[5] G. Laštovička-Medin, M. Rebarz, G. Kramberger, J. Kroll, K. Kropielnicki, T. Laštovička, M. Precek, J. Andreasson, Femtosecond laser studies of the single event effects in low gain avalanche detectors and PINs at ELI beamlines, Nucl. Instrum. Methods Phys. Res. A 1041 (2022) http://dx.doi.org/10.1016/j.nima.2022.167321.

[6] R. Geertsema, K. Akiba, M. van Beuzekom, T. Bischoff, K. Heijhoff, H. Snoek, Charge and temporal characterisation of silicon sensors using a two-photon absorption laser, J. Instrum. 17 (2022) http://dx.doi.org/10.1088/1748-0221/17/02/P02023.
[7] M. Moll, Displacement damage in silicon detectors for high energy physics, IEEE Trans. Nucl. Sci. 65 (8) (2018) http://dx.doi.org/10.1109/TNS.2018.2819506.
[8] FYLA S.L., Spain. URL https://fyla.com/.
[9] A. Almagro-Ruiz, S. Pape, H. Muñoz-Marco, M. Wiehe, E. Currás, M. Fernández-García, M. Moll, R. Montero, F.R. Palomo, C. Quintana, I. Vila, P. Pérez-Millán, Fiber laser system of 1550 nm femtosecond pulses with configurable properties for the two-photon excitation of transient currents in semiconductor detectors, Appl. Opt. 61 (32) (2022) 9386–9397, http://dx.doi.org/10.1364/AO.470780, URL https://opg.optica.org/ao/abstract.cfm?URI=ao-61-32-9386.
[10] Huber Kältemaschinenbau AG, Germany. URL https://www.huber-online.com.
[11] M. Wiehe, Development of a Two-Photon Absorption - TCT System and Study of Radiation Damage in Silicon Detectors (Ph.D. thesis), Albert-Ludwigs-Universit, 2021, URL https://cds.cern.ch/record/2795933.
[12] CIVIDEC TCT amplifier. URL https://cividec.at/index.php?module=public.product&idProduct=35&scr=0.
[13] IMB-CNM-CSIC, Centre Nacional de Microelectrònica, Barcelona, Spain, 2018.
[14] P.H. Wendland, M. Chester, Electric field effects on indirect optical transitions in silicon, Phys. Rev. 140 (1965) http://dx.doi.org/10.1103/PhysRev.140.A1384.
[15] P.A. Tove, W. Seibt, Plasma effects in semiconductor detectors, Nucl. Instrum. Methods 51 (1967) http://dx.doi.org/10.1016/0029-554X(67)90012-2.
[16] F. Palomo, M. Moll, M. Fernández-García, R. Montero, I. Vila, Plasma effects in silicon detectors and the two photon absorption transient current technique, 2021, http://dx.doi.org/10.1109/RADECS53308.2021.9954488.
[17] J. Bardeen, W. Shockley, Deformation potentials and mobilities in non-polar crystals, Phys. Rev. 80 (1950) 72–80, http://dx.doi.org/10.1103/PhysRev.80.72, URL https://link.aps.org/doi/10.1103/PhysRev.80.72.
[18] S. Sze, K. Ng, Physics of Semiconductor Devices, third ed., 2007.
[19] H.H. Li, Refractive index of silicon and germanium and its wavelength and temperature derivatives, J. Phys. Chem. Ref. Data 9 (1980) http://dx.doi.org/10.1063/1.555624.
[20] S. Pape, M. Fernández García, M. Moll, R. Montero, F. Palomo, I. Vila, M. Wiehe, Characterisation of irradiated and non-irradiated silicon sensors with a table-top two photon absorption TCT system, J. Instrum. 17 (08) (2022) C08011, http://dx.doi.org/10.1088/1748-0221/17/08/c08011.
[21] J. Becker, E. Fretwurst, R. Klanner, Measurements of charge carrier mobilities and drift velocity saturation in bulk silicon of 111 and 100 crystal orientation at high electric fields, Solid-State Electron. 56 (2011) http://dx.doi.org/10.1016/j.sse.2010.10.009.
[22] E. Curras Rivera, Advanced silicon sensors for future collider experiments. Sensores de silicio avanzados para futuros experimentos colisionadores, 2017, URL https://cds.cern.ch/record/2291517.
[23] E. Currás, M. Fernández, M. Moll, Gain suppression mechanism observed in low gain avalanche detectors, Nucl. Instrum. Methods Phys. Res. A (2022) http://dx.doi.org/10.1016/j.nima.2022.166530.
[24] G.F. Sinclair, N.A. Tyler, D. Sahin, J. Barreto, M.G. Thompson, Temperature dependence of the Kerr nonlinearity and two-photon absorption in a silicon waveguide at 1.55 μm, Phys. Rev. Appl. 11 (2019) http://dx.doi.org/10.1103/PhysRevApplied.11.044084.
[25] Y. Varshni, Temperature dependence of the energy gap in semiconductors, Physica 34 (1967) http://dx.doi.org/10.1016/0031-8914(67)90062-6.
[26] T.R. Hart, R.L. Aggarwal, B. Lax, Temperature dependence of Raman scattering in silicon, Phys. Rev. B 1 (1970) http://dx.doi.org/10.1103/PhysRevB.1.638.
[27] M.A. Green, Self-consistent optical parameters of intrinsic silicon at 300K including temperature coefficients, Sol. Energy Mater. Sol. Cells 92 (11) (2008) 1305–1310, http://dx.doi.org/10.1016/j.solmat.2008.06.009, URL https://www.sciencedirect.com/science/article/pii/S0927024808002158.